Journal of Cosmology and Astroparticle Physics
An IOP and SISSA journal

Prospects of detecting dark matter through cosmic-ray antihelium with the antiproton constraints

Yu-Chen Ding, Nan Li, Chun-Cheng Wei, Yue-Liang Wu and Yu-Feng Zhou

CAS Key Laboratory of Theoretical Physics,
Institute of Theoretical Physics, Chinese Academy of Sciences,
Zhongguancun East Rd. 55, Beijing 100190, China
University of Chinese Academy of Sciences,
Yuquan Rd. 19A, Beijing 100049, China
E-mail: dingyucheng@itp.ac.cn, linan2016@itp.ac.cn, ccwei@itp.ac.cn, ylwu@itp.ac.cn, yfzhou@itp.ac.cn

Received March 25, 2019
Accepted May 20, 2019
Published June 3, 2019

Abstract. Cosmic-ray (CR) antihelium is an important observable for dark matter (DM) indirect searches due to extremely low secondary backgrounds towards low energies. In a given DM model, the predicted CR antihelium flux is expected to be strongly correlated with that of CR antiprotons. In this work, we use the AMS-02 $\bar{p}/p$ data to constrain the DM annihilation cross section, and the ALICE data on the $^3\overline{\mathrm{He}}$ and $\overline{\mathrm{T}}$ productions to determine the parameters in the coalescence model for anti-nucleus formation. The hadronic cross sections are estimated using Monte-Carlo event generators including `EPOS-LHC` and `DPMJET`. Based on these constraints, we make predictions for the maximal antihelium flux for typical DM annihilation final states, and perform a detailed analysis on the uncertainties due to the DM density profiles and CR propagation models. We find that the results are highly insensitive to both of them, but still significantly depend on the hadronization models in event generators. The prospects of detecting antihelium for the AMS-02 experiment is discussed. We show that with very optimistic assumptions, CR $^3\overline{\mathrm{He}}$ is within the reach of the AMS-02 experiment. The $^3\overline{\mathrm{He}}$ events which can be detected by AMS-02 are likely to have kinetic energy $T \gtrsim 30\,\mathrm{GeV}$, which is consistent with the preliminary AMS-02 search results. The events which can be observed by AMS-02 are likely to arise dominantly from secondary backgrounds rather than DM interactions.

Keywords: dark matter experiments, dark matter theory

ArXiv ePrint: 1808.03612

https://doi.org/10.1088/1475-7516/2019/06/004

JCAP06(2019)004

Contents

1 Introduction

Although the existence of dark matter (DM) as the dominant component of matter in the present-day Universe has been well established by observations, the particle nature of DM remains largely unknown. If DM particles in the Galactic halo can annihilate or decay into the standard model (SM) stable final states, they can make extra contributions to the fluxes of cosmic-ray (CR) particles, which can be probed by high precision DM indirect search experiments. Among many CR observables, CR antimatter, such as CR positrons, antiprotons and heavier anti-nuclei such as antideuteron and antihelium are considered to be relatively rare as they are dominated by CR secondaries produced by the collisions of primary CR particles onto the interstellar gas. Thus CR antiparticles are expected to be sensitive to extra contributions and can be important probes of DM interactions.

In recent years, a number of experiments including AMS-02 have confirmed an unexpected rise in the CR positron flux above $\sim$10 GeV [1–4]. DM annihilation or decay can be a possible explanation to this phenomena (see e.g. refs. [5–8] for discussions related to the AMS-02 data) which is, however, subject to stringent constraints such as that from the observations of γ-rays from dwarf galaxies [9], the Galactic center [10], and the measurement of anisotropy in the cosmological microwave background (CMB) [11]. Another important observable is the CR antiproton which has been measured by a number of experiments such as PAMELA [12], BESS-polar II [13] and AMS-02 [14]. The high precision measurement of AMS-02 shows that in a large rigidity range from $\sim$ 1 to 450 GV, the antiproton flux is in an overall agreement with the secondary origin of CR antiprotons, which can be used to place stringent constraints on the properties of DM particles (see e.g. refs. [15–18]).

Despite tiny production rates, heavier anti-nuclei such as antideuteron ($\overline{\mathrm{D}}$) and antihelium-3 ($^3\overline{\mathrm{He}}$) can also be important probes of DM, and can be searched by the experiments such as BESS [19], AMS-02 [20, 21] and GAPS [22]. With the increase of the atomic mass number A, the fluxes of anti-nuclei are expected to decrease rapidly due to smaller volume of phase space for the formation of anti-nuclei for both DM annihilation and secondary production. However, the fluxes of secondary anti-nuclei are further suppressed

JCAP06(2019)004

in the low-energy region as the final state anti-nuclei are highly boosted due to the high production thresholds in pp-collisions ($17m_p$ for $\overline{\mathrm{D}}$ and $31m_p$ for $^3\overline{\mathrm{He}}$, where m_p is the proton mass). The extremely low background makes it easier to single out the DM contributions in the low energy region below $\sim$10 GeV. Furthermore, at very high energies the secondary production is suppressed by the rapid falling of the primary CR flux at high energies (the CR proton flux scales with energy E as $E^{-2.75}$).

CR antideuteron production from DM interactions has been extensively discussed (for a recent review, see e.g. [23]). The CR antihelium production was first discussed in [24, 25]. It has been noticed that in a given DM model, the predicted fluxes of antiproton and antideuteron should be correlated. Thus the constraints from the antiproton data can be used to set limits on the maximal fluxes of antideuteron [26–28]. The same strategy can be applied to the case of CR antihelium production, which was briefly discussed in [29] based on a fixed DM profile and CR propagation model and the value of coalescence momentum p_0 in the coalescence model for antinucleon formation inferred from rescaling the value for antideuteron.

In this work, we perform an updated analysis on the prospects of detecting $^3\overline{\mathrm{He}}$ events in the AMS-02 experiment, motivated partly by the recent progresses in searching for heavier anti-nuclei made by AMS-02 [30]. We use the AMS-02 $\bar{p}/p$ data to constrain the DM annihilation cross sections, taking into account the uncertainties in DM profiles and CR propagation models, and use the ALICE antinuclei production data from pp-collisions to directly constrain p_0 for various Monte-Carlo (MC) hadronization event generators including `PYTHIA`, `EPOS-LHC` and `DPMJET`. Based on these constraints, we make predictions for the maximal antihelium flux for typical DM annihilation final states. We find that the resulting predictions for the maximal fluxes of $^3\overline{\mathrm{He}}$ are highly insensitive to the choice of DM profiles and propagation models, due to the fact that the variation in the DM density profile and propagation model mainly leads to a rescaling of the DM annihilation cross sections in such a way that the same antiproton flux is reproduced. The results, however, are still significantly depends on the hadronization models in the MC event generators. We show that with very optimistic estimations of detection efficiency and acceptance, CR $^3\overline{\mathrm{He}}$ is within the sensitivity of the AMS-02 experiment with a whole lifetime of data taking. Furthermore, We find that the events which can be detected by AMS-02 first are likely to have kinetic energy $T \gtrsim 30$ GeV, which is consistent with the very preliminary AMS-02 antihelium measurements [30]. However, they should dominantly arise from secondary backgrounds rather than DM annihilation.

This paper is organized as follows: in section 2, we give a brief overview of the coalescence model for the formation of heavy anti-neuclei. In section 3, we use the ALICE antinuclei production data from pp-collisions to directly constrain p_0 for various MC event generators `PYTHIA 8.2`, `EPOS-LHC` and `DPMJET-III` for hadronization, and discuss the energy spectra of $^3\overline{\mathrm{He}}$ in the cases of DM annihilation and pp-collisions. In section 4, we constrain the DM annihilation cross section using the AMS-02 $\bar{p}/p$ ratio data. In section 5, we calculate the $^3\overline{\mathrm{He}}$ flux at the top of atmosphere and discuss the detection prospect of the AMS-02 experiment. The conclusions of this work are summarized in section 6.

2 The coalescence model

We adopt the coalescence model [31–33] to describe the formation of an anti-nuclei $\bar{\mathrm{A}}$ from anti-nucleons. In this model a single parameter of coalescence momentum $p_0^{\bar{\mathrm{A}}}$ is introduced to determine whether the anti-nucleons produced in a collision process can merge into an anti-nucleus. The basic assumption is that the anti-nucleons are able to merge into an anti-

JCAP06(2019)004

nucleus only if a proper combination of the relative four-momenta of the constituent nucleons is less than $p_0^{\bar{\rm A}}$. For instance, in the case of antideuteron formation, the coalescence criterion is defined as

$$||k_{\bar{p}} - k_{\bar{n}}|| = \sqrt{(\Delta\vec{k})^2 - (\Delta E)^2} < p_0^{\bar{\rm D}}, \tag{2.1}$$

where $k_{\bar{p}}$ and $k_{\bar{n}}$ are the four-momenta of $\bar{p}$ and $\bar{n}$ respectively, and $p_0^{\bar{\rm D}}$ is the coalescence momentum of antideuteron. In the case where the momentum distributions of $\bar{p}$ and $\bar{n}$ are isotropic and statistically independent, the energy spectrum of $\bar{\rm D}$ is related to that of $\bar{p}$ and $\bar{n}$ as

$$\gamma_{\bar{\rm D}}\frac{d^3N_{\bar{\rm D}}}{d^3\vec{k}_{\bar{\rm D}}}(\vec{k}_{\bar{\rm D}}) = \frac{\pi}{6}\left(p_0^{\bar{\rm D}}\right)^3 \cdot \gamma_{\bar{p}}\frac{d^3N_{\bar{p}}}{d^3\vec{k}_{\bar{p}}}(\vec{k}_{\bar{p}}) \cdot \gamma_{\bar{n}}\frac{d^3N_{\bar{n}}}{d^3\vec{k}_{\bar{n}}}(\vec{k}_{\bar{n}}), \tag{2.2}$$

where $\gamma_{\bar{\rm D},\bar{p},\bar{n}}$ are the Lorentz factors, and $\vec{k}_{\bar{p}} \approx \vec{k}_{\bar{n}} \approx \vec{k}_{\bar{\rm D}}/2$.

The coalescence criterion for the heavier anti-nuclei can be defined in a similar way as that of antideuteron [24, 25]. For the case of $^3\overline{\rm He}$, one can define the norms of the relative four-momenta between the three anti-nucleons as three lengths $l_1 = ||k_1 - k_2||$, $l_2 = ||k_2 - k_3||$ and $l_3 = ||k_1 - k_3||$, where k_1, k_2, k_3 are the four-momenta of the three anti-nucleons respectively. one can use these lengths to compose a triangle, and then make a circle to envelope the triangle with a minimal diameter. It is assumed that the three anti-nucleons can successfully merge into an anti-nucleus only if the diameter of the circle is less than $p_0^{\overline{\rm He}}$ [24]. If the three lengths form a right or obtuse triangle (i.e., $l_i^2 + l_j^2 \leqslant l_m^2$, for any i, j, m), the minimal diameter equals to the longest side of the triangle, then the criterion can be simply written as $\max\{l_1, l_2, l_3\} < p_0^{\overline{\rm He}}$. On the other hand, if the three lengths form an acute triangle ($l_i^2 + l_j^2 > l_m^2$, for all i, j, m), the minimal circle is just the circumcircle of this triangle. In this case, the criterion can be expressed in terms of the diameter of the circumcircle

$$d_{\rm circ} = \frac{l_1 l_2 l_3}{\sqrt{(l_1 + l_2 + l_3)(-l_1 + l_2 + l_3)(l_1 - l_2 + l_3)(l_1 + l_2 - l_3)}} < p_0^{\overline{\rm He}}. \tag{2.3}$$

An alternative way to define the coalescence criterion for $^3\overline{\rm He}$ is simply requiring that the relative four-momentum of each pair of the constituent anti-nuclei is smaller than $p_0^{\overline{\rm He}}$ [25]:

$$||k_i - k_j|| < p_0^{\overline{\rm He}}, \qquad (i \neq j). \tag{2.4}$$

If the relative four-momenta form a right or obtuse triangle, This method is equivalent to the method of eq. (2.3), namely, $p_0^{\overline{\rm He}}$ is determined by the longest side of the triangle. However, for the case of acute triangles, this method predicts slightly more anti-nuclei. The quantitative difference between these two methods will be discussed in the next section.

The spatial positions of particles also play an important role in the formation of anti-nuclei, one should exclude the particle pairs which are not close enough to each other in space. As shown in ref. [24], this can be taken into account by setting all the particles with lifetime $\tau \gtrsim 2$ fm/c to be stable, where 2 fm is approximately the size of the $^3\overline{\rm He}$ nucleus.

3 Coalescence momentum for antiHelium formation from the ALICE data

The value of $p_0^{\bar{\rm A}}$ can be constrained by collider data. For instance, in the case of antideuteron production, the value of $p_0^{\bar{\rm D}}$ can be determined by reproducing the ALEPH measurement of the process $e^+e^- \to \overline{\rm D} + X$ at the Z^0 resonance [34]. An analysis based on the Monte-Carlo (MC) event generator `PYTHIA` gave $p_0^{\bar{\rm D}} = 0.192 \pm 0.030$ GeV [26]. The value of $p_0^{\bar{\rm D}}$ is known

JCAP06(2019)004

to be slightly dependent on the center-of-mass (CM) energy and the collision process [23, 35]. As summarized in ref. [23], other collider experiments at different center-of-mass (CM) energies lead to different values of p_0 in the range $\sim 0.13-0.24\,\mathrm{GeV}$ [36–41]. Considering the resemblance to the dynamics of the annihilation of DM, we shall use the value of $p_0^{\overline{\mathrm{D}}}$ derived from the ALEPH data as a benchmark value.

For the case of antihelium production, as the experimental data are rare, it has been proposed to estimate the value of $p_0^{\overline{\mathrm{He}}}$ based on that of $p_0^{\overline{\mathrm{D}}}$. Two methods have been considered in literature [24]. The first one is to use the averaged ratio of $p_0^{A=3}/p_0^{A=2}$ through fitting the inclusive spectra of deuterons, tritons and ^{3}He from the data on AA-collisions at the Berkeley Bevalac collider [42], and then assume the relation $p_0^{\overline{\mathrm{He}}}/p_0^{\overline{\mathrm{D}}} \approx \langle p_0^{A=3}/p_0^{A=2}\rangle$, which leads to

$$p_0^{\overline{\mathrm{He}}} \approx \langle p_0^{A=3}/p_0^{A=2}\rangle\; p_0^{\bar{\mathrm{D}}} = 1.28\; p_0^{\bar{\mathrm{D}}} = 0.246 \pm 0.038\ \mathrm{GeV}. \tag{3.1}$$

The second one is to use the theoretical scaling relation $p_0 \sim \sqrt{E_b}$ [43], where E_b is the total nuclear binding energy, and obtain

$$p_0^{\overline{\mathrm{He}}} \approx p_0^{\bar{\mathrm{D}}} \sqrt{E_b^{^3\overline{\mathrm{He}}}/E_b^{\overline{\mathrm{D}}}} = 0.357 \pm 0.059\ \mathrm{GeV}. \tag{3.2}$$

In recent years, direct production of antihelium/antitriton have been observed in pp-collisions [35, 40, 44] and AA-collisions at high CM energies [45, 46]. These experiments measured the phenomenological coalescence parameter B_A defined through the relation

$$E_A \frac{d^3N_A}{dp_A^3} = B_A \left(E_p \frac{d^3N_p}{dp_p^3}\right)^Z \left(E_n \frac{d^3N_n}{dp_n^3}\right)^N, \quad \vec{p}_p = \vec{p}_n = \vec{p}_A/A, \tag{3.3}$$

where A is the nucleus mass number, Z the proton number and N the neutron number with $A = Z + N$. In the isotropic limit, it is expected that $B_A \approx p_0^{3(A-1)}$ from the phase-space analysis. The ALICE experiment measured the parameter B_3 for $^3\overline{\mathrm{He}}$ production in three transverse momentum bins $p_T/A = 0.4$–$0.6\,\mathrm{GeV}$, 0.6–1.0 GeV and 1.0–2.0 GeV, respectively, with rapidity $|y| < 0.5$ at a CM energy $\sqrt{s} = 7\,\mathrm{TeV}$ in pp-collisions [44]. The B_3 parameter for $\overline{\mathrm{T}}$ production was measured in a single p_T bin $p_T/A = 0.4$–$0.6\,\mathrm{GeV}$. The corresponding coalescence momenta were determined based on the values of B_3 using an interpolation approach in which the relation $B_A \approx p_0^{3(A-1)}$ was assumed.

As the real collision process could be different significantly from the isotropic limit, we adopt an alternative approach in the determination of the coalescence momenta without assuming $B_A \approx p_0^{3(A-1)}$. For a given MC event generator, we generate a large sample of $\mathcal{O}(10^{11})$ pp-collision events and keep record of the momentum information of the final states $\bar{p}/\bar{n}$ which have the potential to form an $^3\overline{\mathrm{He}}$ or $\overline{\mathrm{T}}$ nucleus, namely, selecting the $\bar{p}/\bar{n}$ particles according to a sufficiently large coalescence momentum $p_{0,\mathrm{max}} = 1\,\mathrm{GeV}$. We then allow the value of p_0 to vary freely in the range $p_0 < p_{0,\mathrm{max}}$ and use the condition of eq. (2.3) for antinucleus formation within the sample to fit the measured values of B_3. We perform χ^2-fits for three MC event generators: `PYTHIA 8.2` [47, 48], `EPOS-LHC` [49, 50] and `DPMJET-III` [51]. Another popular event generator is `QGS-JET` [52, 53]. It was shown in ref. [54] that after some tuning of the parameters for better fit the low-energy collider data, the results from `QGS-JET` is similar to that from `EPOS-LHC`. The fit results are summarized in table 1. The uncertainties in the determined coalescence momenta arise from the uncertainties in the ALICE data, which are typically around 10% or less. Although our approach is quite different from that adopted by the ALICE collaboration, we find that both results are in reasonable agreement with each other.

JCAP06(2019)004

MC generators:	PYTHIA 8.2	EPOS-LHC	DPMJET-III
$p_0^{\overline{\mathrm{He}}}$ (MeV)	224^{+12}_{-16} (254 ± 14)	227^{+11}_{-16} (254 ± 14)	212^{+10}_{-13}
$p_0^{\overline{\mathrm{T}}}$ (MeV)	234^{+17}_{-29} (266 ± 22)	245^{+17}_{-30} (268 ± 22)	222^{+16}_{-26}

Table 1. Best-fit values of $p_0^{\overline{\mathrm{He}}}$ and $p_0^{\overline{\mathrm{T}}}$ from fitting to the ALICE data of pp-collision at $\sqrt{s} = 7\,\mathrm{TeV}$ for three MC generators PYTHIA 8.2 [47, 48], EPOS-LHC [49, 50] and DPMJET-III [51]. The numbers in the brackets are the values obtained by the ALICE collaboration using an interpolation approach [44].

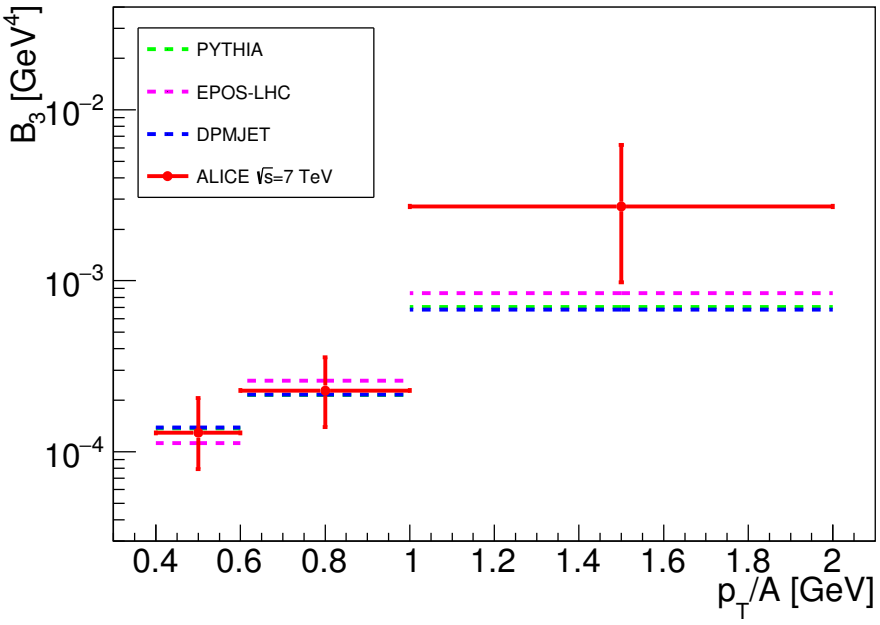

Figure 1. Best-fit values of the B_3 parameter from fitting to the ALICE data of pp-collision in three p_T bins, for three MC generators PYTHIA 8.2, EPOS-LHC and DPMJET-III, respectively. The ALICE data are also shown [44].

In figure 1 we show the best-fit values of B_3 for ${}^3\overline{\mathrm{He}}$ formation in three p_T bins. The χ^2-curves of the fit results are shown in the left panel of figure 2. In all the fits, we find $\chi^2_{\mathrm{min}}/\mathrm{d.o.f} \lesssim 0.6/2$, indicating reasonable agreement with the ALICE data. The figure also shows that the coalescence model can well reproduce the p_T-dependence of B_3 in the low p_T bins. At the highest p_T bin $p_T/A = 1.0 - 2.0\,\mathrm{GeV}$, the coalescence model predict a slightly lower value. For the case of $\overline{\mathrm{T}}$ production, the ALICE data is perfectly reproduced as it is only available for a single p_T bin. The corresponding χ^2-curves are shown in the right pannel of figure 2.

An ${}^3\overline{\mathrm{He}}$ nucleus can be formed directly from the coalescence of $\bar{p}\bar{p}\bar{n}$, or through the β-decay of an antitriton $\overline{\mathrm{T}}$ ($\bar{p}\bar{n}\bar{n}$). Compared with the formation of $\overline{\mathrm{T}}$, the direct formation channel is expected to be suppressed by Coulomb-repulsion between the two antiprotons. The suppression effect is, however, difficult to estimate quantitatively. From table 1, it can be seen that the determined coalescence momenta for ${}^3\overline{\mathrm{He}}$ are only slightly smaller than that for $\overline{\mathrm{T}}$ by $\sim (5 - 10)\%$, suggesting that the effect of Coulomb-repulsion may not be

JCAP06(2019)004

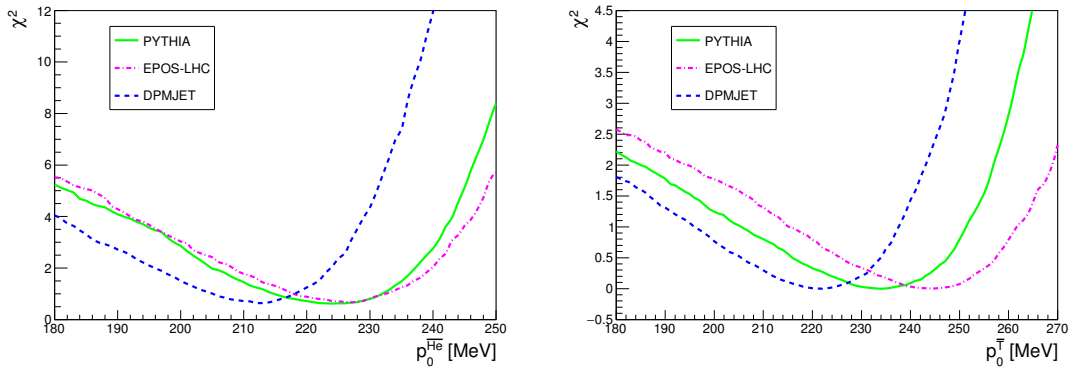

Figure 2. Left) Values of χ^2 as a function of the coalescence momentum $p_0^{\overline{\mathrm{He}}}$ from fitting to the ALICE data [44] for three MC event generators. Right) the same as left but for the coalescence momentum $p_0^{\overline{\mathrm{T}}}$.

significant, which is consistent with the analysis in ref. [55]. In the following calculations, we shall include the contributions from $\overline{\mathrm{T}}$ using the corresponding B_3 values, and approximate the energy spectrum of $^3\overline{\mathrm{He}}$ from the decay of $\overline{\mathrm{T}}$ to be the same as that of $\overline{\mathrm{T}}$ for a given production process, which roughly enhance the final $^3\overline{\mathrm{He}}$ number by a factor of two or three depending on the production processes.

For the DM interaction induced primary $^3\overline{\mathrm{He}}$, we use `PYTHIA 8.2` to simulate the hadronization processes of DM annihilation, and adopt the coalescence model to describe the $^3\overline{\mathrm{He}}$ formation on an event-by-event basis. In `PYTHIA`, the DM annihilation process $\chi\chi \to f\bar{f}$ (where f stands for any SM particle) is mimicked by a process of electron-positron annihilation through a fictious singlet scalar $e^+e^- \to \phi^* \to f\bar{f}$ with a center-of-mass energy $\sqrt{s} = 2m_\chi$ and *all* the initial-state-radiations switched off, which guarantees that the initial states are color-neutral and not interfere with the final state interactions of the SM particles. Other MC event generators, such as `EPOS-LHC` and `DPMJET`, etc., only use hadrons as initial states, which are not appropriate to simulate the DM annihilation in a straightforward way. We consider two Majorana DM particles annihilating into $q\bar{q}$ (q stands for u or d quark), $b\bar{b}$ and W^+W^- final states. Four possible values for the DM particle mass are considered, m_χ= 30, 100, 300, and 1000 GeV. We generate $\mathcal{O}(10^{11})$ events for each case of DM particle mass to produce enough $^3\overline{\mathrm{He}}$ particles for calculating the injection energy spectrum. The final number of $^3\overline{\mathrm{He}}$ particles produced is around $\mathcal{O}(10^4)$ for all the cases. In figure 3, we show the obtained energy spectra of $^3\overline{\mathrm{He}}$ per DM annihilation as a function of the scaled kinetic energy per nucleon $x = T/(Am_\chi)$. As can be seen from figure 3, for $q\bar{q}$ or $b\bar{b}$ channels, increasing the DM mass always leads to higher $^3\overline{\mathrm{He}}$ yields and softer spectrum due to the longer chain of parton showers. However, for W^+W^- final states, the spectrum becomes harder. The reason is that for the heavier DM, the produced W^+W^- particles are more energetic, and the decay products of W^+W^- are boosted to higher energies, which lead to the decrease of $^3\overline{\mathrm{He}}$ towards lower energies. In order to quantitatively discuss the difference between the two coalescence criterions in eqs. (2.3) and (2.4), we perform a test for the case of m_χ = 1000 GeV with $q\bar{q}$ final states, and found that the method of eq. (2.3) produces about 13% fewer $^3\overline{\mathrm{He}}$ particles compares to the method of eq. (2.4). The difference found in our calculation is larger than the previous estimation of $\sim 6\%$ in ref. [24] which assumed an isotropic momenta distribution. Nevertheless, the difference between the two methods would not affect the conclusion qualitatively.

JCAP06(2019)004

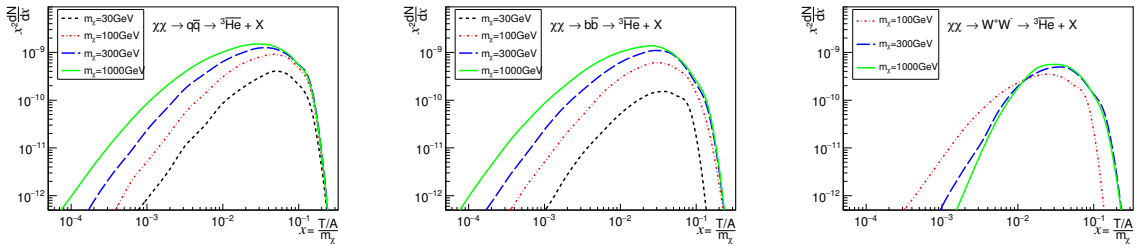

Figure 3. Energy spectra of CR $^3\overline{\mathrm{He}}$ from DM annihilation as a function of scaled kinetic energy per nucleon $x = T/(Am_\chi)$ in the center-of-mass frame for different DM particle masses $m_\chi = 30 - 1000\,\mathrm{GeV}$. The left, middle and right panels correspond to $q\bar{q}$, $b\bar{b}$ and W^+W^- annihilation channels, respectively. The events are generated using `PYTHIA 8.2` [47, 48].

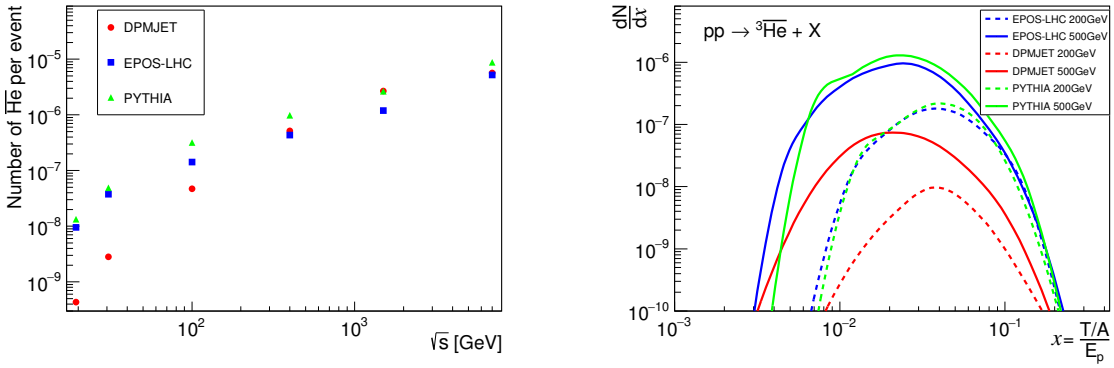

Figure 4. Left) Total number of $^3\overline{\mathrm{He}}$ events from pp-collisions at different center-of-mass energies. The events are generated using three event generators `PYTHIA 8.2`, `EPOS-LHC` and `DPMJET-III`. Right) Energy spectra of $^3\overline{\mathrm{He}}$ events from pp-collisions in the target-rest frame at two different energies of incident protons $E_{\mathrm{lab}} = 200$ and 500 GeV for the three MC event generators.

For the secondary $^3\overline{\mathrm{He}}$ productions from pp-collisions, we shall use the MC event generators `EPOS-LHC` and `DPMJET-III` to simulate the production of anti-nucleons and the coalescence model to estimate the formation of $^3\overline{\mathrm{He}}$. The difference between the two MC event generators can be used as a rough estimation of the uncertainties related to hadronization models. The default parameters in `PYTHIA 8.2` (i.e. the Monash tune [56]) is not optimized for pp-collisions at relatively low energies. We anyway include the results from `PYTHIA 8.2` for a comparison purpose. In the left panel of figure 4, we show the total number of $^3\overline{\mathrm{He}}$ events at different CM energies for the three event generators. At CM energies around a few tens of GeV which is most relevant to the secondary $^3\overline{\mathrm{He}}$ production, `PYTHIA 8.2` and `EPOS-LHC` give similar results while `DPMJET-III` predict significantly lower number of $^3\overline{\mathrm{He}}$ events. For instance, at $\sqrt{s} = 30\,\mathrm{GeV}$, the difference between `EPOS-LHC` and `DPMJET-III` can reach an order of magnitude. The energy spectra obtained for the three event generators at two different energies of incident protons $E_{\mathrm{lab}} = 200$ and 500 GeV (corresponds to $\sqrt{s}$=19.4 and 30.7 GeV, respectively) in the target rest frame are shown in the right panel of figure 4. As it can be seen from the figure, although the coalescence momentum of $^3\overline{\mathrm{He}}$ production in all the event generators are calibrated to the same ALICE pp-collision data at $\sqrt{s} = 7\,\mathrm{TeV}$, at lower CM energies, the predicted $^3\overline{\mathrm{He}}$ energy spectrum can be significantly different.

JCAP06(2019)004

4 Updated limits from AMS-02 antiproton data

4.1 Cosmic-ray propagation

The propagation of CR anti-nuclei in the Galaxy can be described by a diffusion model in which the diffusion zone is assumed to be a cylinder with radius $r_h \approx 20$ kpc and half-height $z_h = 1 \sim 10$ kpc. The diffusion equation of CR charged particles can be written as [57, 58]:

$$\frac{\partial f}{\partial t} = q(\vec{r}, p) + \nabla \cdot (D_{xx} \nabla f - \vec{V}_c f) + \frac{\partial}{\partial p} p^2 D_{pp} \frac{\partial}{\partial p} \frac{f}{p^2} - \frac{\partial}{\partial p} \left[\dot{p} f - \frac{p}{3} (\nabla \cdot \vec{V}_c) f \right] - \frac{f}{\tau_f} - \frac{f}{\tau_r} , \quad (4.1)$$

where $f(\vec{r}, p, t)$ is the number density per unit of particle momentum p at the position $\vec{r}$, and $q(\vec{r}, p)$ is the source term. D_{xx} is the energy-dependent spatial diffusion coefficient which is parameterized as $D_{xx} = \beta D_0 (R/R_0)^{\delta}$, where $R = p/(Ze)$ is the rigidity of the cosmic-ray particle with electric charge Ze, δ is the spectral power index which can take two different values $\delta = \delta_{1(2)}$ when R is below (above) a reference rigidity R_0, D_0 is a constant normalization coefficient, and $\beta = v/c$ is the velocity of CR particles. $\vec{V}_c$ is the convection velocity, which is related to the galactic wind. Diffusive re-acceleration is described as diffusion in momentum space, and is described by the parameter D_{pp} which can be parameterized as $D_{pp} = 4V_a^2 p^2/(3D_{xx}\delta(4-\delta^2)(4-\delta))$, where V_a is the Alfvèn velocity which characterises the propagation of weak disturbances in a magnetic field. $\dot{p} \equiv dp/dt$ is the momentum loss rate, τ_f and τ_r are the time scales of particle fragmentation and radioactive decay respectively. The steady-state diffusion condition is achieved by setting $\partial f/\partial t = 0$. For the boundary conditions, it is assumed that the number densities of CR particles are vanishing at the boundary of the halo: $f(r_h, z, p) = f(r, \pm z_h, p) = 0$. We use the code `GALPROP v54` [59–63] to solve the diffusion equation of eq. (4.1) numerically.

The source term in the propagation equation describe the creation of CR particles. For the primary anti-nuclei $\bar{A}$ ($\bar{A} = \bar{p}, {}^3\overline{\mathrm{He}}$) produced by the annihilation of Majorana DM particles, the source term can be written as follows:

$$q_{\bar{A}}(\vec{r}, p) = \frac{\rho_{\mathrm{DM}}^2(\vec{r})}{2m_\chi^2} \langle \sigma v \rangle \frac{dN_{\bar{A}}}{dp} , \quad (4.2)$$

where $\rho_{\mathrm{DM}}(\vec{r})$ is the DM energy density, $\langle \sigma v \rangle$ is the thermally-averaged annihilation cross section of DM and $dN_{\bar{A}}/dp$ is the energy spectrum of $\bar{A}$ discussed in the previous section.

The source term for the secondary $\bar{A}$ is given by

$$q_{\bar{A}}(\vec{r}, p) = \sum_{ij} n_j(\vec{r}) \int \beta_i \, c \, \sigma_{ij \to \bar{A}}^{\mathrm{inel}}(p') \frac{dN_{\bar{A}}(p, p')}{dp} \, n_i(\vec{r}, p') \, dp' , \quad (4.3)$$

where n_i is the number density of CR proton/Helium (or antiproton) per unit momentum, n_j is the number density of the interstellar hydrogen/Helium, and $\sigma_{ij}^{\mathrm{inel}}(p')$ is the inelastic cross section for the process $ij \to \bar{A} + X$. $dN_{\bar{A}}(p, p')/dp$ is the energy spectrum of $\bar{A}$ in the collision with the momentum of the incident CR particle denoted by p'. For the source term of $\bar{p}$, we include the collisions of pp, pHe, Hep, HeHe, $\bar{p}p$ and $\bar{p}$He. For the source of ${}^3\overline{\mathrm{He}}$, since the B_3 data are only available in pp-collisions, we consider the contribution form pp-collisions which dominates the secondary background of ${}^3\overline{\mathrm{He}}$.

The energy spectrum of $\bar{p}$ can be obtained through some parameterization formulae based on scaling behaviors with the involved parameters determined by the low energy pp-collision data [64–67], or using MC event generators [54, 68]. The difference between the

JCAP06(2019)004

two approaches can reach a factor of a few [54]. The MC event generators can simulate the jet-structure of the final state partons which is very important for the formation of heavy nuclei. In this work, for consistency, we shall use the MC event generators for both the secondary $\bar{p}$ and $^3\overline{\rm He}$ production from pp-collisions.

The primary CR nucleus injection spectra are assumed to have a broken power law behavior $f_p(\vec{r}, p) \propto p^{\gamma_p}$, with the injection index $\gamma_p = \gamma_{p1}(\gamma_{p2})$ for the nucleus rigidity R_p below (above) a reference value R_{ps}. The spatial distribution of the interstellar gas and the primary sources of CR nuclei are taken from ref. [59]. In the case of $\bar{p}$ production, the tertiary contributions are included. However, in the case of the $^3\overline{\rm He}$ production, the sub-dominant tertiary contributions are neglected, as they are only compatible with the secondary background at kinetic energies below $0.4 - 0.6\,{\rm GeV/A}$ [69].

The inelastic interaction rate $\Gamma_{\rm int}$ of the scattering between the nucleus $\bar{A}$ and the interstellar gas is related to the fragmentation scale τ_f in eq. (4.1) as $\Gamma_{\rm int} = 1/\tau_f$, and can be estimated as [24, 25]

$$\Gamma_{\rm int} = (n_{\rm H} + 4^{2/3} n_{\rm He})\; v\; \sigma_{\bar{A}p}\,, \tag{4.4}$$

where $n_{\rm H}$ and $n_{\rm He}$ are the number densities of interstellar hydrogen and helium, respectively, $4^{2/3}$ is the geometrical factor, v is the velocity of $\bar{A}$ relative to interstellar gases, and $\sigma_{\overline{\rm He}p}$ is the total inelastic cross section for the collisions between $\bar{A}$ and the interstellar gas. The number density ratio He/H in the interstellar gas is taken to be 0.11 [59].

Since the experimental data of the cross section $\sigma_{\overline{\rm He}p}$ is currently not available, we assume the relation $\sigma_{\bar{A}p} = \sigma_{A\bar{p}}$ by CP-invariance. For an incident nucleus with atomic mass number A, charge number Z and kinetic energy T, the total inelastic cross section for $A\bar{p}$ collision is parameterized by the following formula [60]

$$\sigma^{\rm tot}_{A\bar{p}} = A^{2/3}\left[48.2 + 19\,x^{-0.55} + (0.1 - 0.18\,x^{-1.2})Z + 0.0012\,x^{-1.5}Z^2\right]\ {\rm mb}, \tag{4.5}$$

where $x = T/(A \cdot {\rm GeV})$. For instance, by substituting $A = 3$ and $Z = 2$, one obtains the cross section $\sigma_{\overline{\rm He}p}$.

Finally, when anti-nuclei propagate into the heliosphere, the magnetic fields of the solar system and the solar wind can distort the spectrum of the charged CR particles. We use the force-field approximation [70] to quantify the effects of solar modulation

$$\Phi^{\rm TOA}_{A,Z}(T_{\rm TOA}) = \left(\frac{2m_A T_{\rm TOA} + T^2_{\rm TOA}}{2m_A T_{\rm IS} + T^2_{\rm IS}}\right)\Phi^{\rm IS}_{A,Z}(T_{\rm IS}), \tag{4.6}$$

where Φ stands for the flux of the CR particles, which is related to the density function f by $\Phi = vf/(4\pi)$, "TOA" stands for the value at the top of the atmosphere of the earth, "IS" stands for the value at the boundary between the interstellar and the heliosphere and m is the mass of the nucleus. $T_{\rm IS}$ is related to $T_{\rm TOA}$ as $T_{\rm IS} = T_{\rm TOA} + e\phi_F|Z|$. In this work, the value of the Fisk potential is fixed at $\phi_F = 550$ MV.

4.2 Updated upper limits on DM annihilation cross sections from AMS-02 antiproton data

The DM annihilation cross sections for annihilation channels such as $\chi\chi \to q\bar{q}$, $b\bar{b}$ and W^+W^- are subject to the constraints from CR antiproton data, the constraints are expected to be strongly correlated with the predictions for the maximal $^3\overline{\rm He}$ flux. In ref. [16], upper limits on DM annihilation cross sections were obtained based on the preliminary AMS-02 $\bar{p}/p$ data

JCAP06(2019)004

Model	r_h(kpc)	z_h(kpc)	D_0	R_0(GV)	δ_1/δ_2	V_a(km/s)	R_{ps}(GV)	γ_{p1}/γ_{p2}
MIN	20	1.8	3.53	4.0	0.3/0.3	42.7	10.0	1.75/2.44
MED	20	3.2	6.50	4.0	0.29/0.29	44.8	10.0	1.79/2.45
MAX	20	6.0	10.6	4.0	0.29/0.29	43.4	10.0	1.81/2.46

Table 2. Values of the main parameters in the "MIN", "MED" and "MAX" models derived from fitting to the AMS-02 B/C and proton data based on the `GALPROP` code [72]. The parameter D_0 is in units of 10^{28} cm$^2 \cdot$ s^{-1}.

JCAP06(2019)004

released in 2015 [71] and the background estimated from the parametrization of Tan and Ng [64]. In this work, we update the analysis by using the latest AMS-02 $\bar{p}/p$ [14] and use MC event generators for calculating antiproton production cross sections.

In order to take into account the uncertainties in CR propagation, we consider three representative propagation models, the "MIN", "MED" and "MAX" models [72]. These models were obtained from a global fit to the CR proton and B/C data of AMS-02 using the `GALROP-v54` code, which represents the typically minimal, median and maximal antiproton fluxes due to the uncertainties in propagation models. Note that these models are different from the ones proposed in ref. [73] which are based on semi-analytical solutions of the propagation equation. The values of parameters for the three models are listed in table 2. In this updated analysis, the primary nuclei source term is normalized to reproduce the AMS-02 proton flux at a reference kinetic energy $T = 100$ GeV, which is the default normalization scheme in `GALPROP`.

For each propagation model, four commonly used DM density profiles are considered: the Navarfro-Frenk-White (NFW) profile [74], the Isothermal profile [75], the Moore profile [76, 77] and the Einasto profile [78]. The upper limits on the DM annihilation cross section as a function of DM particle mass are derived using the frequentist χ^2-analyses. The expression of χ^2 is defined as $\chi^2 = \sum_i (f_i^{\rm th} - f_i^{\rm exp})^2/\sigma_i^2$, where $f_i^{\rm th}$ are the theoretical predictions, $f_i^{\rm exp}$ and σ_i are the central values and errors of experimental data, respectively. The index i runs over all the available data points. For a given DM particle mass, we first calculate the minimal value $\chi^2_{\rm min}$ of the χ^2-function, and then derive the 95% CL upper limits on the annihilation cross section, corresponding to $\Delta\chi^2 = 3.84$ for one parameter. More details of deriving the upper limits can be found in ref. [16]. The obtained limits for $q\bar{q}$, $b\bar{b}$ and W^+W^- channels are presented in figure 5 and figure 6, together with the secondary background estimated by `EPOS-LHC` and `DPMJET-III`, respectively.

We find that the updated upper limits are comparable with the previous ones, but the constraints for $m_\chi \lesssim 100$ GeV become more stringent, which is partly due to larger cross sections from `EPOS-LHC` and `DPMJET-III` and the updated AMS-02 data. For a comparison, in figures 5–6, the upper limits from the Fermi-LAT 6-year gamma-ray data of the dwarf spheroidal galaxies [9] are also shown. With the growth of the DM mass, the upper limits become weaker, and can be well above the typical thermal relic cross section $\langle\sigma v\rangle = 3 \times 10^{-26}$ cm$^3 \cdot$ s^{-1} for $m_\chi \gtrsim 100$ GeV. The upper limits for $\chi\chi \to q\bar{q}$ channel are the most stringent among the three types of final states. For the "MED" and the "MAX" model, the obtained upper limits are comparable with that from the Fermi-LAT γ-ray data.

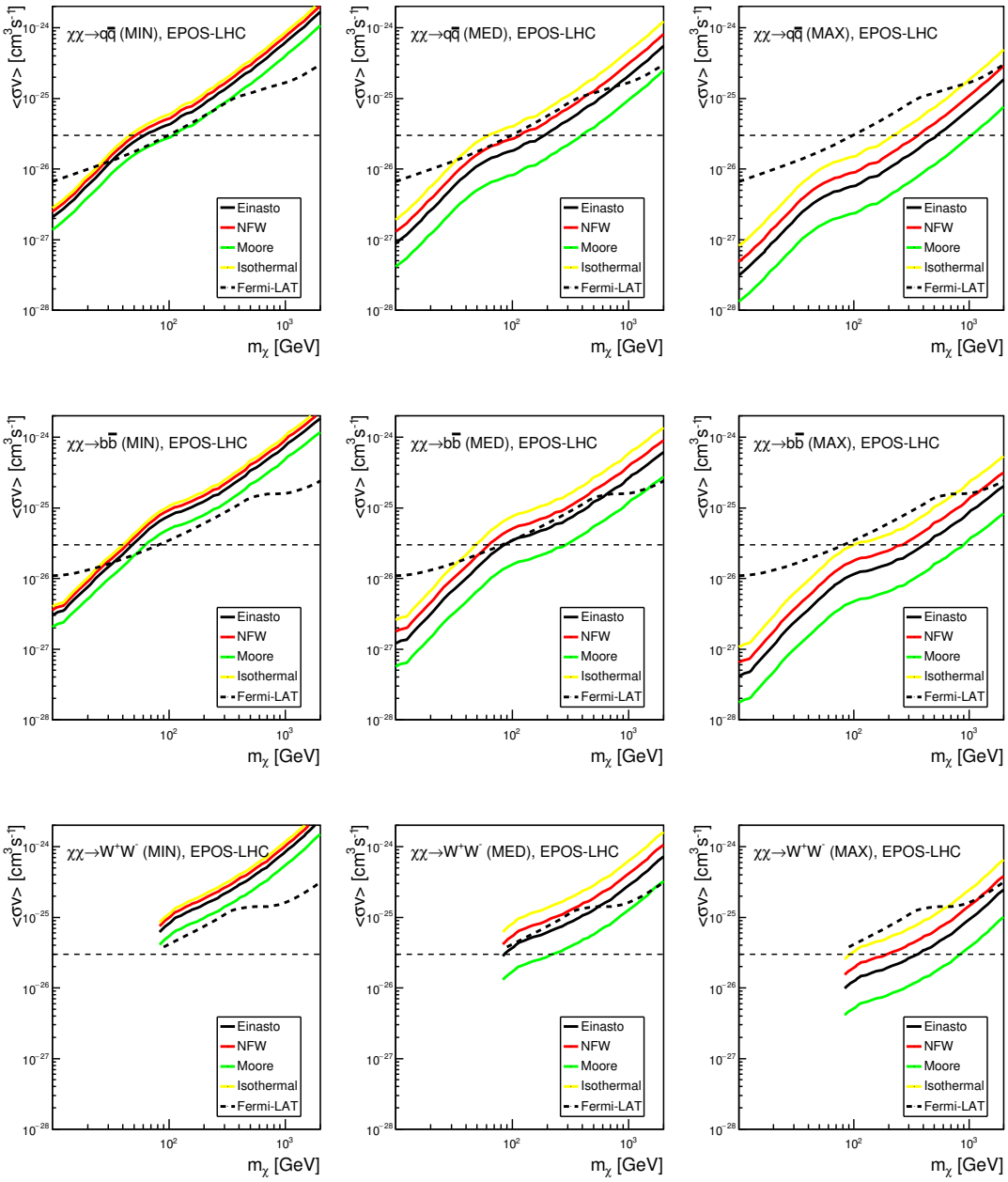

Figure 5. 95% C.L. upper limits on DM annihilation cross sections for different annihilation channels, propagation models and DM profiles. The secondary backgrounds are estimated using MC event generator `EPOS-LHC`.

5 Prospects of detecting $^3\overline{\mathrm{He}}$ events at AMS-02

After obtaining the upper limits on the DM annihilation cross sections, it is straight forward to discuss the prospects of detecting $^3\overline{\mathrm{He}}$ in current and future experiments. The major source of uncertainties in the prediction for $^3\overline{\mathrm{He}}$ fluxes involves: i) the uncertainties in the choice of DM density profiles. For a fixed DM annihilation cross section, the variation in the

JCAP06(2019)004

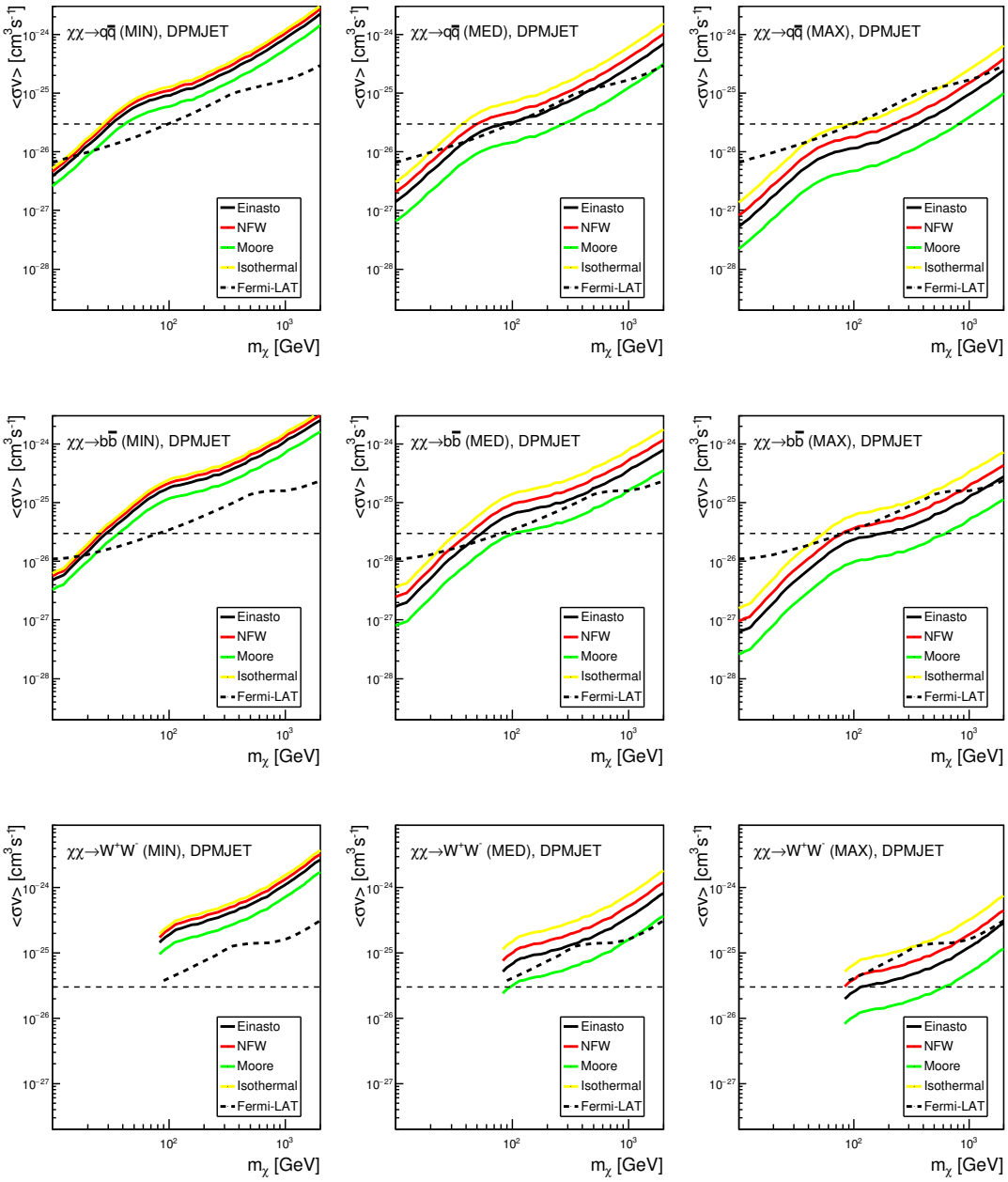

Figure 6. The same as figure 5, but with the secondary backgrounds estimated by DPMJET-III.

choice of DM profiles from the NFW profile to the isotheramal profile can lead to a change in the final $^3\overline{\text{He}}$ flux up to an order of magnitude. ii) the uncertainties in the choice of different propagation models. As shown in the previous works [24, 25], it can change the predicted flux of $^3\overline{\text{He}}$ up to two orders of magnitude for a given DM annihilation cross section. iii) the uncertainties in the modeling of $^3\overline{\text{He}}$ formation. As the current data of $^3\overline{\text{He}}$ production are only available at high CM energies around TeV scale, the MC event generators calibrated to the same high-energy data may give quite different predictions at low energies. From the

JCAP06(2019)004

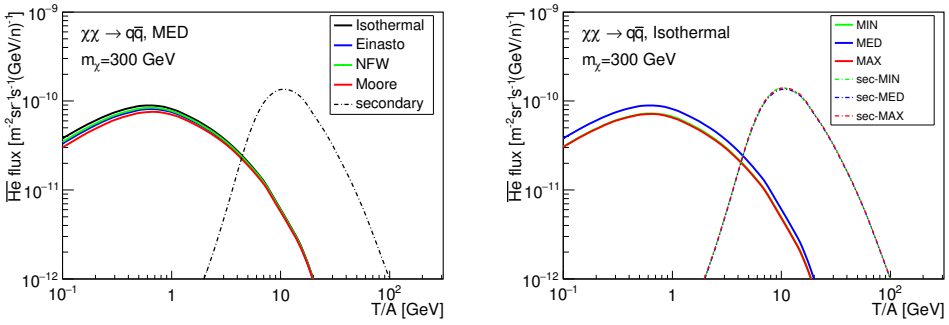

Figure 7. Left) Predicted maximal $^3\overline{\text{He}}$ fluxes (solid curves) as a function of kinetic energy per nucleon from DM annihilation into $q\bar{q}$ final states in the MED propagation model with four different DM profiles NFW [74], Isothermal [75], Einasto [78] and Moore [76, 77]. The DM particle mass is fixed at $m_\chi = 300\,\text{GeV}$. The secondary $^3\overline{\text{He}}$ fluxes generated by `EPOS-LHC` are also shown for a comparison. Right) The same as left, but for three different propagation models MIN, MED and MAX [72] with DM profile fixed to "Isothermal".

left panel of figure 4, the differences between the MC event generators can reach an order of magnitude. iv) The uncertainties in the coalescence momentum $p_0^{\overline{\text{He}}}$. The production rate of $^3\overline{\text{He}}$ is approximately proportional to $(p_0^{\overline{\text{He}}})^6$. Thus an uncertainty of $\sim 10\%$ in p_0 can be amplified to $\sim 60\%$ in the predicted antihelium flux.

An great advantage of using the antiproton data to constrain the predictions for $^3\overline{\text{He}}$ flux is that the obtained constraints become highly insensitive to the choice of DM density profile, as varying the DM profile mainly results in a rescaling of the best-fit $\langle\sigma v\rangle$ in such a way that the same antiproton flux is reproduced. In the left panel of figure 7, we show the prediction for the maximal $^3\overline{\text{He}}$ flux after constrained by the AMS-02 CR antiproton data for the four different DM profiles in the same MED propagation model for DM particles with mass fixed at 300 GeV and $q\bar{q}$ the dominant annihilation final states. Compared with figure 5 and figure 6, it can be seen that for the four DM profiles, the difference in the constraints on the DM annihilation cross sections can reach $\mathcal{O}(10)$, while that in the predicted $^3\overline{\text{He}}$ flux are reduced to $\sim 30\%$. Similarly, the predictions become also highly insensitive to the choice of propagation models, provided that they give rise to similar secondary antiproton backgrounds. In the right panel of figure 7, we show the upper limits on $^3\overline{\text{He}}$ flux for the three different propagation models with the same DM profile. For the models giving nearly the same secondary background such as the "MIN", "MED" and "MAX" models, the difference in the predicted $^3\overline{\text{He}}$ flux is also very small $\sim 30\%$.

Detecting CR antihelium is one of the major scientific objectives of the AMS-02 experiment. In this work, we give an estimation of the maximal number of $^3\overline{\text{He}}$ events which can be observed by AMS-02 after taking into account the constraints from the AMS-02 antiproton data. We assume the whole lifetime of the experiment to be 18 years, and adopt the most optimistic assumptions related to the detectors. In general, the number of $^3\overline{\text{He}}$ events observed by a detector can be written as

$$N = \int_{T_{\text{min}}}^{T_{\text{max}}} \eta\, \Phi_{\overline{\text{He}}}\, \mathcal{A}\, t\, dT, \tag{5.1}$$

where $\Phi_{\overline{\text{He}}}$ is the flux of $^3\overline{\text{He}}$, $\mathcal{A}$ is the acceptance of $^3\overline{\text{He}}$ which is assumed to be identical to the geometric acceptance of the AMS-02 detector $\mathcal{A} \approx 0.5\ \text{m}^2 \cdot \text{sr}$, η is the detecting efficiency

JCAP06(2019)004

	m_χ (GeV)	$\chi\chi \to q\bar{q}$	$\chi\chi \to b\bar{b}$	$\chi\chi \to W^+W^-$
DM	30	$0.084^{+0.038}_{-0.040}$ $(0.153^{+0.070}_{-0.073})$	$0.041^{+0.020}_{-0.018}$ $(0.073^{+0.036}_{-0.032})$	—
	100	$0.153^{+0.065}_{-0.072}$ $(0.269^{+0.114}_{-0.127})$	$0.227^{+0.107}_{-0.103}$ $(0.419^{+0.198}_{-0.190})$	$0.164^{+0.077}_{-0.076}$ $(0.304^{+0.143}_{-0.141})$
	300	$0.122^{+0.055}_{-0.056}$ $(0.179^{+0.081}_{-0.082})$	$0.160^{+0.074}_{-0.074}$ $(0.256^{+0.118}_{-0.118})$	$0.054^{+0.025}_{-0.025}$ $(0.084^{+0.039}_{-0.039})$
	1000	$0.106^{+0.048}_{-0.048}$ $(0.138^{+0.063}_{-0.063})$	$0.131^{+0.058}_{-0.061}$ $(0.179^{+0.079}_{-0.083})$	$0.015^{+0.007}_{-0.007}$ $(0.019^{+0.009}_{-0.009})$
Secondary		$0.986^{+0.437}_{-0.455}$ $(0.054^{+0.021}_{-0.021})$		

Table 3. Prospective maximal number of $^3\overline{\text{He}}$ particles with which can be detected by AMS-02 after 18 years of data taking under the most optimistic assumptions. The number of secondary $^3\overline{\text{He}}$ are estimated using MC event generator `EPOS-LHC`. The numbers in the brackets correspond to the results using `DPMJET-III`. The quoted uncertainties are due to that in the coalescence momentum $p_0^{\overline{\text{He}}}$ determined from the ALICE data.

which is assumed to be unity, and $t \approx 18$ yr is the total exposure time of the AMS-02 experiment. The lower and upper limits of the integration are set to be $T_{\min(\max)}/A = 0.1\,\text{GeV}$ (1 TeV).

In table 3, we show the predicted maximal number of antihelium events for the three different annihilation channels and four DM particle masses from 30 GeV to 1 TeV using two MC event generators `EPOS-LHC` and `DPMJET`. The expected secondary backgrounds are also shown for a comparison. We find that in the most optimistic cases, the expected total number of events can reach $\mathcal{O}(1)$, and is very likely to be dominated by the secondaries.

A more realistic estimation of the prospective 18-year $^3\overline{\text{He}}$ detecting sensitivity of AMS-02 after considering the contamination of He was given in terms of $\overline{\text{He}}$/He flux ratio in ref. [21], where He stands for ^{3}He+ ^{4}He. In figure 8, we show the predicted $\overline{\text{He}}$/He in the "MED" propagation model with the "Isothermal" DM profile for various DM annihilation channels, DM particle masses, and coalescence momenta using event generators `EPOS-LHC` and `DPMJET`. We find that the events which can be observed are likely to have kinetic energy $T/A \gtrsim 10\,\text{GeV}$, i.e., $T \gtrsim 30\,\text{GeV}$ for $^3\overline{\text{He}}$, and are dominantly arising from the secondary backgrounds. Recently, the AMS-02 collaboration has reported preliminary hints of antihelium events [79]. For instance, a candidate event of $^3\overline{\text{He}}$ with momentum $40.3 \pm 2.9\,\text{GeV}$ is shown. Such a event corresponds to a kinetic energy per nucleon $T/A \approx 12.5 \pm 1.0\,\text{GeV}$. As can be seen from the upper panels of figure 8, it is close to the overlap region between the AMS-02 sensitivity and the prediction from the secondary production. Thus the energy of the candidate event is consistent with the secondary $^3\overline{\text{He}}$ prediction in the most optimistic case. From figure 8, it is also evident that DM-interaction induced $^3\overline{\text{He}}$ are unlikely to be observed by AMS-02.

For a comparison with the previous work in the literature, in figure 9, our results are compared with a selection of previous work related to the projection of the CR $^3\overline{\text{He}}$ flux. The analysis in ref. [29] considered the constraints form the AMS-02 antiproton data, and used the coalescence model with the `DPMJET-III` event generator to simulate $^3\overline{\text{He}}$ formation. However, the coalescence momentum $p_0^{\overline{\text{He}}}$ was inferred from the vale of $p_0^{\overline{\text{D}}}$, which is quite large $p_0^{\overline{\text{He}}} \approx 311\,\text{MeV}$ and leads to the conclusion that CR $^3\overline{\text{He}}$ is within the reach of AMS-02. On the country, in our work, we use the value $p_0^{\overline{\text{He}}} = 212^{+10}_{-13}\,\text{MeV}$ directly from fitting the ALICE data. Consequently, in our work the predicted CR $^3\overline{\text{He}}$ flux using `DPMJET-III` is an order of magnitude lower. In ref. [55], the coalescence parameter B_3 was estimated using the ALICE data and the Hanbury-Brown-Twiss (HBT) two-particle-correlation measurements. The obtained value of B_3 is in a wide range $(2-20)\times10^{-4}\,\text{GeV}^4$. Consequently, the predicted $^3\overline{\text{He}}$ flux can be much larger than that from other approaches. However, as shown by the

JCAP06(2019)004

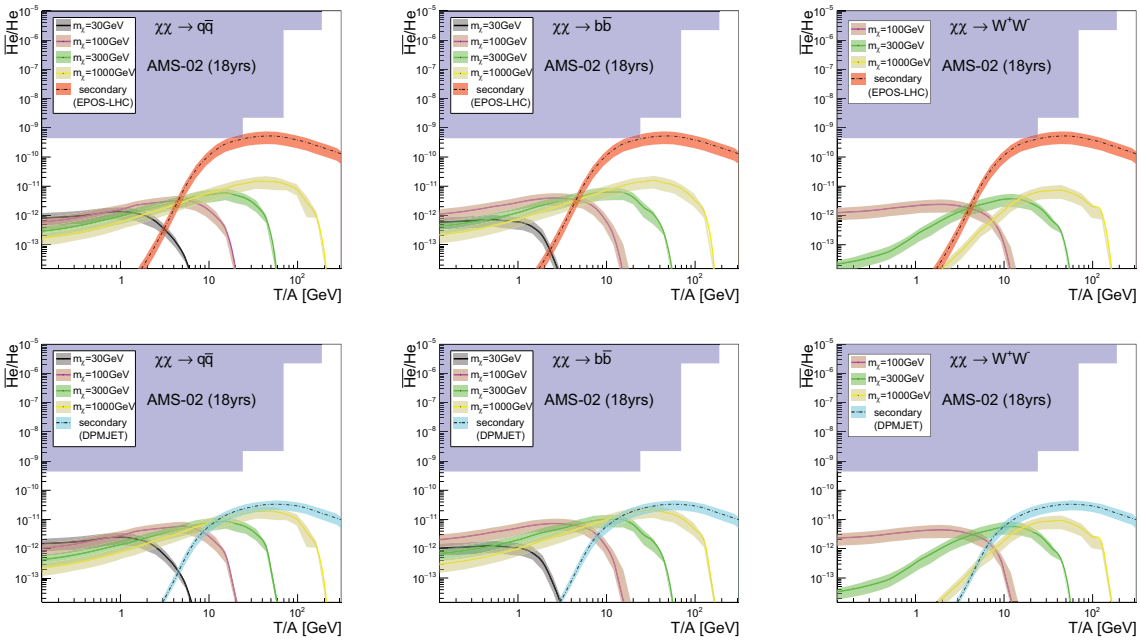

Figure 8. Upper panels) maximal flux ratios $\overline{\text{He}}/\text{He}$ from DM annihilation under the constraints from the AMS-02 $\bar{p}$ data, together with the secondary $^3\overline{\text{He}}$ backgrounds. The pp-collision cross section and the coalescence momentum $p_0^{\overline{\text{He}}}$ are determined using the MC event generator `EPOS-LHC`. The error bands indicate the uncertainty in the coalescence momentum. The results are obtained by adopting the "MED" propagation model and the "Isothermal" DM profile. The blue shaded regions represent the detection sensitivity of AMS-02 at 95% C.L., after 18 years of data collection. Lower panels) the same as the upper panels, but based on the event generator `DPMJET-III`.

ALICE data (see figure 1), the value of B_3 shows a significant p_T dependence which was not reproduced in the HBT approach in [55]. Only in the highest p_T bin the value of B_3 can reach 20×10^{-4} GeV^4. For lower p_T bins, the corresponding B_3 can be smaller by an order of magnitude. Note that the p_T dependence of B_3 is correctly reproduced by the all MC event generators considered in this work. In ref. [69], the maximal $^3\overline{\text{He}}$ flux from DM annihilation was discussed with the AMS-02 antiproton constraints taken directly from ref. [80]. The analysis of [69] used the coalescence model and the analytic relation between $p_0^{\overline{\text{He}}}$ and B_3 in the isotropic limit, which again cannot reproduced the p_T dependence of B_3. To be conservative, the value of $p_0^{\overline{\text{He}}}$ was set in the range $160 - 248$ MeV, which leads to large uncertainties in the predicted maximal $^3\overline{\text{He}}$ flux. The $^3\overline{\text{He}}$ flux from DM was also discussed recently in light of the preliminary antihelium measurements by AMS-02 [81]. However, neither the antiproton constriants nor the background contributions was considered in their analysis.

6 Conclusions

In summary, motivated partly by the recent progresses made by AMS-02 in searching for heavier anti-nuclei, we have discussed the prospect of detecting $^3\overline{\text{He}}$ in the AMS-02 experiment under the constraints from the AMS-02 antiproton data. We have updated the upper limits on DM annihilation cross sections from the AMS-02 $\bar{p}/p$ ratio, and then used the results to set limits on the $^3\overline{\text{He}}$ flux and number of events which could be observed by AMS-02 in the whole lifetime of data taking. We have used the coalescence model to simulate the

JCAP06(2019)004

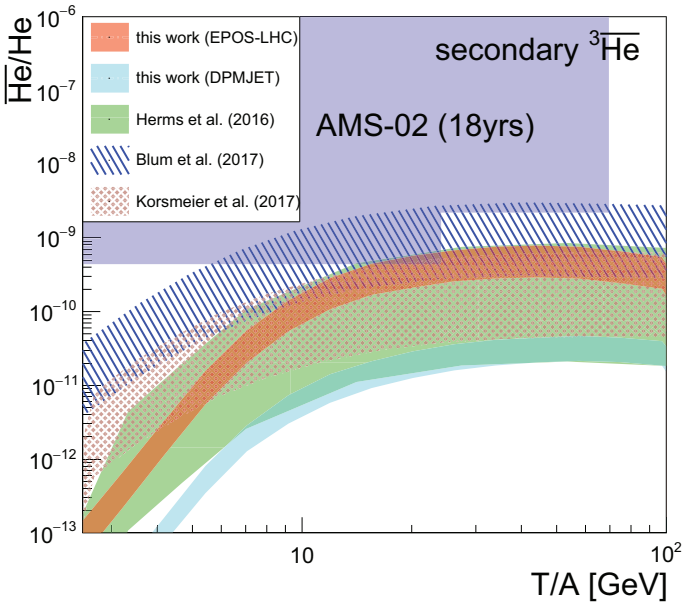

Figure 9. A comparison of the secondary contribution to the flux ratio $^3\overline{\mathrm{He}}$/He obtained in this work with that from the previous work by Herms, et al. [29], Blum, et al. [55] and Korsmeier, et al. [69]. See text for detailed discussions.

production of $^3\overline{\mathrm{He}}$ from DM annihilation on an event-by-event basis, and used the GALPROP code to calculate the propagation of $^3\overline{\mathrm{He}}$ in the interstellar medium. The results show that with very optimistic estimates of detection efficiency and acceptance, and a relatively large coalescence momentum, CR antihelium is within the sensitivity of the AMS-02 experiment with a whole lifetime of data taking. The number of events can reach $\mathcal{O}(1)$, depending on the value of the coalescence momentum. We have also shown that the events which can be detected by AMS-02 are likely to have kinetic energy $T \gtrsim 30\,\mathrm{GeV}$ and dominantly arise from secondary backgrounds rather than DM annihilation.

Acknowledgments

We are grateful to Alejandro Ibarra for useful discussions on the prospect of detecting antihelium at AMS-02. This work is supported in part by the NSFC under Grants No. U1738209, No. 11851303, No. 11825506, No. 11821505, the National Key R&D Program of China No. 2017YFA0402204, and the CAS key research program No. XDB23030100, No. QYZDY-SSW-SYS007.

References

[1] J.J. Beatty et al., *New measurement of the cosmic-ray positron fraction from 5 to 15 GeV*, *Phys. Rev. Lett.* **93** (2004) 241102 [astro-ph/0412230] [INSPIRE].

[2] PAMELA collaboration, *An anomalous positron abundance in cosmic rays with energies 1.5–100 GeV*, *Nature* **458** (2009) 607 [arXiv:0810.4995] [INSPIRE].

[3] FERMI-LAT collaboration, *Measurement of separate cosmic-ray electron and positron spectra with the Fermi Large Area Telescope*, *Phys. Rev. Lett.* **108** (2012) 011103 [arXiv:1109.0521] [INSPIRE].

JCAP06(2019)004

[4] AMS collaboration, *High statistics measurement of the positron fraction in primary cosmic rays of* 0.5–500 *GeV with the Alpha Magnetic Spectrometer on the International Space Station*, *Phys. Rev. Lett.* **113** (2014) 121101 [INSPIRE].

[5] J. Kopp, *Constraints on dark matter annihilation from AMS-02 results*, *Phys. Rev.* **D 88** (2013) 076013 [arXiv:1304.1184] [INSPIRE].

[6] L. Bergstrom, T. Bringmann, I. Cholis, D. Hooper and C. Weniger, *New limits on dark matter annihilation from AMS cosmic ray positron data*, *Phys. Rev. Lett.* **111** (2013) 171101 [arXiv:1306.3983] [INSPIRE].

[7] A. Ibarra, A.S. Lamperstorfer and J. Silk, *Dark matter annihilations and decays after the AMS-02 positron measurements*, *Phys. Rev.* **D 89** (2014) 063539 [arXiv:1309.2570] [INSPIRE].

[8] H.-B. Jin, Y.-L. Wu and Y.-F. Zhou, *Implications of the first AMS-02 measurement for dark matter annihilation and decay*, *JCAP* **11** (2013) 026 [arXiv:1304.1997] [INSPIRE].

[9] FERMI-LAT and DES collaborations, *Searching for dark matter annihilation in recently discovered milky way satellites with Fermi-LAT*, *Astrophys. J.* **834** (2017) 110 [arXiv:1611.03184] [INSPIRE].

[10] H.E.S.S. collaboration, *Search for dark matter annihilations towards the inner galactic halo from* 10 *years of observations with H.E.S.S.*, *Phys. Rev. Lett.* **117** (2016) 111301 [arXiv:1607.08142] [INSPIRE].

[11] PLANCK collaboration, *Planck* 2015 *results. XIII. Cosmological parameters*, *Astron. Astrophys.* **594** (2016) A13 [arXiv:1502.01589] [INSPIRE].

[12] O. Adriani et al., *Measurement of the flux of primary cosmic ray antiprotons with energies of* 60 *MeV to* 350 *GeV in the PAMELA experiment*, *JETP Lett.* **96** (2013) 621 [*Pisma Zh. Eksp. Teor. Fiz.* **96** (2012) 693] [INSPIRE].

[13] K. Abe et al., *Measurement of the cosmic-ray antiproton spectrum at solar minimum with a long-duration balloon flight over Antarctica*, *Phys. Rev. Lett.* **108** (2012) 051102 [arXiv:1107.6000] [INSPIRE].

[14] AMS collaboration, *Antiproton flux, antiproton-to-proton flux ratio and properties of elementary particle fluxes in primary cosmic rays measured with the Alpha Magnetic Spectrometer on the International Space Station*, *Phys. Rev. Lett.* **117** (2016) 091103 [INSPIRE].

[15] G. Giesen et al., *AMS-02 antiprotons, at last! Secondary astrophysical component and immediate implications for dark matter*, *JCAP* **09** (2015) 023 [arXiv:1504.04276] [INSPIRE].

[16] H.-B. Jin, Y.-L. Wu and Y.-F. Zhou, *Upper limits on dark matter annihilation cross sections from the first AMS-02 antiproton data*, *Phys. Rev.* **D 92** (2015) 055027 [arXiv:1504.04604] [INSPIRE].

[17] S.-J. Lin, X.-J. Bi, J. Feng, P.-F. Yin and Z.-H. Yu, *Systematic study on the cosmic ray antiproton flux*, *Phys. Rev.* **D 96** (2017) 123010 [arXiv:1612.04001] [INSPIRE].

[18] A. Reinert and M.W. Winkler, *A precision search for WIMPs with charged cosmic rays*, *JCAP* **01** (2018) 055 [arXiv:1712.00002] [INSPIRE].

[19] K. Abe et al., *Search for antihelium with the BESS-polar spectrometer*, *Phys. Rev. Lett.* **108** (2012) 131301 [arXiv:1201.2967] [INSPIRE].

[20] AMS collaboration, *Cosmic rays antideuteron sensitivity for AMS-02 experiment*, in *Proceedings,* 30$^{\text{th}}$ *International Cosmic Ray Conference (ICRC* 2007*)*, vol. 4, Merida, Yucatan, Mexico, 3–11 July 2007, pg. 765.

[21] A. Kounine, *Status of the AMS experiment*, arXiv:1009.5349 [INSPIRE].

[22] GAPS collaboration, *Antideuteron sensitivity for the GAPS experiment*, *Astropart. Phys.* **74** (2016) 6 [arXiv:1506.02513] [INSPIRE].

JCAP06(2019)004

[23] T. Aramaki et al., *Review of the theoretical and experimental status of dark matter identification with cosmic-ray antideuterons*, *Phys. Rept.* **618** (2016) 1 [arXiv:1505.07785] [INSPIRE].

[24] E. Carlson, A. Coogan, T. Linden, S. Profumo, A. Ibarra and S. Wild, *Antihelium from dark matter*, *Phys. Rev.* **D 89** (2014) 076005 [arXiv:1401.2461] [INSPIRE].

[25] M. Cirelli, N. Fornengo, M. Taoso and A. Vittino, *Anti-helium from dark matter annihilations*, *JHEP* **08** (2014) 009 [arXiv:1401.4017] [INSPIRE].

[26] A. Ibarra and S. Wild, *Prospects of antideuteron detection from dark matter annihilations or decays at AMS-02 and GAPS*, *JCAP* **02** (2013) 021 [arXiv:1209.5539] [INSPIRE].

[27] N. Fornengo, L. Maccione and A. Vittino, *Dark matter searches with cosmic antideuterons: status and perspectives*, *JCAP* **09** (2013) 031 [arXiv:1306.4171] [INSPIRE].

[28] S.-J. Lin, X.-J. Bi and P.-F. Yin, *Expectations of the cosmic antideuteron flux*, arXiv:1801.00997 [INSPIRE].

[29] J. Herms, A. Ibarra, A. Vittino and S. Wild, *Antideuterons in cosmic rays: sources and discovery potential*, *JCAP* **02** (2017) 018 [arXiv:1610.00699] [INSPIRE].

[30] S. Ting, *The AMS experiment*, in *AMS days at La Palma*, Instituto de Astrofísica de Canarias, La Palma, Spain, 9 April 2018.

[31] S.T. Butler and C.A. Pearson, *Deuterons from high-energy proton bombardment of matter*, *Phys. Rev.* **129** (1963) 836 [INSPIRE].

[32] A. Schwarzschild and C. Zupancic, *Production of tritons, deuterons, nucleons and mesons by 30 GeV protons on A1, Be and Fe targets*, *Phys. Rev.* **129** (1963) 854 [INSPIRE].

[33] L.P. Csernai and J.I. Kapusta, *Entropy and cluster production in nuclear collisions*, *Phys. Rept.* **131** (1986) 223 [INSPIRE].

[34] ALEPH collaboration, *Deuteron and anti-deuteron production in e^+e^- collisions at the Z resonance*, *Phys. Lett.* **B 639** (2006) 192 [hep-ex/0604023] [INSPIRE].

[35] ALICE collaboration, *Production of light nuclei and anti-nuclei in pp and Pb-Pb collisions at energies available at the CERN Large Hadron Collider*, *Phys. Rev.* **C 93** (2016) 024917 [arXiv:1506.08951] [INSPIRE].

[36] CLEO collaboration, *Anti-deuteron production in $\Upsilon(nS)$ decays and the nearby continuum*, *Phys. Rev.* **D 75** (2007) 012009 [hep-ex/0612019] [INSPIRE].

[37] BABAR collaboration, *Antideuteron production in $\Upsilon(nS)$ decays and in $e^+e^- \to q\bar{q}$ at $\sqrt{s} \approx 10.58$ GeV*, *Phys. Rev.* **D 89** (2014) 111102 [arXiv:1403.4409] [INSPIRE].

[38] B. Alper et al., *Large angle production of stable particles heavier than the proton and a search for quarks at the CERN intersecting storage rings*, *Phys. Lett.* **B 46** (1973) 265 [INSPIRE].

[39] BRITISH-SCANDINAVIAN-MIT collaboration, *Production of deuterons and anti-deuterons in proton proton collisions at the CERN ISR*, *Lett. Nuovo Cim.* **21** (1978) 189 [INSPIRE].

[40] ALICE collaboration, *Production of nuclei and antinuclei in pp and Pb-Pb collisions with ALICE at the LHC*, *J. Phys.* **G 38** (2011) 124189 [arXiv:1109.4836] [INSPIRE].

[41] ZEUS collaboration, *Measurement of (anti)deuteron and (anti)proton production in DIS at HERA*, *Nucl. Phys.* **B 786** (2007) 181 [arXiv:0705.3770] [INSPIRE].

[42] M.-C. Lemaire, S. Nagamiya, S. Schnetzer, H. Steiner and I. Tanihata, *Composite particle emission in high-energy heavy ion collisions*, *Phys. Lett.* **B 85** (1979) 38 [INSPIRE].

[43] P. Chardonnet, J. Orloff and P. Salati, *The production of antimatter in our galaxy*, *Phys. Lett.* **B 409** (1997) 313 [astro-ph/9705110] [INSPIRE].

JCAP06(2019)004

[44] ALICE collaboration, *Production of deuterons, tritons, ^{3}He nuclei and their antinuclei in pp collisions at $\sqrt{s} = 0.9$, 2.76 and 7 TeV*, *Phys. Rev.* **C 97** (2018) 024615 [arXiv:1709.08522] [INSPIRE].

[45] STAR collaboration, *Anti-deuteron and anti-^{3}He production in $\sqrt{s_{NN}} = 130$ GeV Au+Au collisions*, *Phys. Rev. Lett.* **87** (2001) 262301 [*Erratum ibid.* **87** (2001) 279902] [nucl-ex/0108022] [INSPIRE].

[46] STAR collaboration, *Observation of the antimatter helium-4 nucleus*, *Nature* **473** (2011) 353 [*Erratum ibid.* **475** (2011) 412] [arXiv:1103.3312] [INSPIRE].

[47] T. Sjöstrand, S. Mrenna and P.Z. Skands, *PYTHIA* 6.4 *physics and manual*, *JHEP* **05** (2006) 026 [hep-ph/0603175] [INSPIRE].

[48] T. Sjöstrand et al., *An introduction to PYTHIA* 8.2, *Comput. Phys. Commun.* **191** (2015) 159 [arXiv:1410.3012] [INSPIRE].

[49] K. Werner, F.-M. Liu and T. Pierog, *Parton ladder splitting and the rapidity dependence of transverse momentum spectra in deuteron-gold collisions at RHIC*, *Phys. Rev.* **C 74** (2006) 044902 [hep-ph/0506232] [INSPIRE].

[50] T. Pierog, I. Karpenko, J.M. Katzy, E. Yatsenko and K. Werner, *EPOS LHC: test of collective hadronization with data measured at the CERN Large Hadron Collider*, *Phys. Rev.* **C 92** (2015) 034906 [arXiv:1306.0121] [INSPIRE].

[51] S. Roesler, R. Engel and J. Ranft, *The event generator DPMJET-III at cosmic ray energies*, in 27$^{\text{th}}$ *International Cosmic Ray Conference (ICRC 2001)*, Hamburg, Germany, 7–15 August 2001, pg. 439 [INSPIRE].

[52] S. Ostapchenko, *QGSJET-II: towards reliable description of very high energy hadronic interactions*, *Nucl. Phys. Proc. Suppl.* **151** (2006) 143 [hep-ph/0412332] [INSPIRE].

[53] S. Ostapchenko, *Nonlinear screening effects in high energy hadronic interactions*, *Phys. Rev.* **D 74** (2006) 014026 [hep-ph/0505259] [INSPIRE].

[54] M. Kachelriess, I.V. Moskalenko and S.S. Ostapchenko, *New calculation of antiproton production by cosmic ray protons and nuclei*, *Astrophys. J.* **803** (2015) 54 [arXiv:1502.04158] [INSPIRE].

[55] K. Blum, K.C.Y. Ng, R. Sato and M. Takimoto, *Cosmic rays, antihelium and an old navy spotlight*, *Phys. Rev.* **D 96** (2017) 103021 [arXiv:1704.05431] [INSPIRE].

[56] P. Skands, S. Carrazza and J. Rojo, *Tuning PYTHIA* 8.1*: the Monash* 2013 *tune*, *Eur. Phys. J.* **C 74** (2014) 3024 [arXiv:1404.5630] [INSPIRE].

[57] V.S. Berezinsky, S.V. Bulanov, V.A. Dogiel and V.S. Ptuskin, *Astrophysics of cosmic rays*, North-Holland, Amsterdam, Netherlands (1990) [INSPIRE].

[58] A.W. Strong, I.V. Moskalenko and V.S. Ptuskin, *Cosmic-ray propagation and interactions in the galaxy*, *Ann. Rev. Nucl. Part. Sci.* **57** (2007) 285 [astro-ph/0701517] [INSPIRE].

[59] A.W. Strong and I.V. Moskalenko, *Propagation of cosmic-ray nucleons in the galaxy*, *Astrophys. J.* **509** (1998) 212 [astro-ph/9807150] [INSPIRE].

[60] I.V. Moskalenko, A.W. Strong, J.F. Ormes and M.S. Potgieter, *Secondary anti-protons and propagation of cosmic rays in the galaxy and heliosphere*, *Astrophys. J.* **565** (2002) 280 [astro-ph/0106567] [INSPIRE].

[61] A.W. Strong and I.V. Moskalenko, *Models for galactic cosmic ray propagation*, *Adv. Space Res.* **27** (2001) 717 [astro-ph/0101068] [INSPIRE].

[62] I.V. Moskalenko, A.W. Strong, S.G. Mashnik and J.F. Ormes, *Challenging cosmic ray propagation with antiprotons. Evidence for a fresh nuclei component?*, *Astrophys. J.* **586** (2003) 1050 [astro-ph/0210480] [INSPIRE].

JCAP06(2019)004

[63] V.S. Ptuskin, I.V. Moskalenko, F.C. Jones, A.W. Strong and V.N. Zirakashvili, *Dissipation of magnetohydrodynamic waves on energetic particles: impact on interstellar turbulence and cosmic ray transport*, *Astrophys. J.* **642** (2006) 902 [astro-ph/0510335] [INSPIRE].

[64] L.C. Tan and L.K. Ng, *Calculation of the equilibrium anti-proton spectrum*, *J. Phys.* **G 9** (1983) 227 [INSPIRE].

[65] R.P. Duperray, C.Y. Huang, K.V. Protasov and M. Buenerd, *Parameterization of the antiproton inclusive production cross-section on nuclei*, *Phys. Rev.* **D 68** (2003) 094017 [astro-ph/0305274] [INSPIRE].

[66] M. di Mauro, F. Donato, A. Goudelis and P.D. Serpico, *New evaluation of the antiproton production cross section for cosmic ray studies*, *Phys. Rev.* **D 90** (2014) 085017 [*Erratum ibid.* **D 98** (2018) 049901] [arXiv:1408.0288] [INSPIRE].

[67] M. Korsmeier, F. Donato and M. Di Mauro, *Production cross sections of cosmic antiprotons in the light of new data from the NA*61 *and LHCb experiments*, *Phys. Rev.* **D 97** (2018) 103019 [arXiv:1802.03030] [INSPIRE].

[68] M. Kachelriess, I.V. Moskalenko and S.S. Ostapchenko, *Nuclear enhancement of the photon yield in cosmic ray interactions*, *Astrophys. J.* **789** (2014) 136 [arXiv:1406.0035] [INSPIRE].

[69] M. Korsmeier, F. Donato and N. Fornengo, *Prospects to verify a possible dark matter hint in cosmic antiprotons with antideuterons and antihelium*, *Phys. Rev.* **D 97** (2018) 103011 [arXiv:1711.08465] [INSPIRE].

[70] L.J. Gleeson and W.I. Axford, *Solar modulation of galactic cosmic rays*, *Astrophys. J.* **154** (1968) 1011 [INSPIRE].

[71] S. Ting, *Introduction to the AMS experiment*, in *AMS*-02 *days at CERN*, CERN, Geneva, Switzerland, 15–17 April 2015.

[72] H.-B. Jin, Y.-L. Wu and Y.-F. Zhou, *Cosmic ray propagation and dark matter in light of the latest AMS*-02 *data*, *JCAP* **09** (2015) 049 [arXiv:1410.0171] [INSPIRE].

[73] F. Donato, N. Fornengo, D. Maurin and P. Salati, *Antiprotons in cosmic rays from neutralino annihilation*, *Phys. Rev.* **D 69** (2004) 063501 [astro-ph/0306207] [INSPIRE].

[74] J.F. Navarro, C.S. Frenk and S.D.M. White, *A universal density profile from hierarchical clustering*, *Astrophys. J.* **490** (1997) 493 [astro-ph/9611107] [INSPIRE].

[75] L. Bergstrom, P. Ullio and J.H. Buckley, *Observability of gamma-rays from dark matter neutralino annihilations in the milky way halo*, *Astropart. Phys.* **9** (1998) 137 [astro-ph/9712318] [INSPIRE].

[76] B. Moore et al., *Dark matter substructure within galactic halos*, *Astrophys. J.* **524** (1999) L19 [astro-ph/9907411] [INSPIRE].

[77] J. Diemand, B. Moore and J. Stadel, *Convergence and scatter of cluster density profiles*, *Mon. Not. Roy. Astron. Soc.* **353** (2004) 624 [astro-ph/0402267] [INSPIRE].

[78] J. Einasto, *Dark matter*, in *Astronomy and astrophysics* 2010, O. Engvold, R. Stabell, B. Czerny and J. Lattanzio eds., in *Encyclopedia of Life Support Systems (EOLSS)*, developed under the auspices of the UNESCO, Eolss Publishers, Oxford, U.K. (2009) [arXiv:0901.0632] [INSPIRE].

[79] S. Ting, *The first five years of the Alpha Magnetic Spectrometer on the International Space Station*, in *CERN Colloquium*, CERN, Geneva, Switzerland, 8 December 2016.

[80] A. Cuoco, M. Krämer and M. Korsmeier, *Novel dark matter constraints from antiprotons in light of AMS*-02, *Phys. Rev. Lett.* **118** (2017) 191102 [arXiv:1610.03071] [INSPIRE].

[81] A. Coogan and S. Profumo, *Origin of the tentative AMS antihelium events*, *Phys. Rev.* **D 96** (2017) 083020 [arXiv:1705.09664] [INSPIRE].

JCAP06(2019)004